19th CIRP Conference on Modeling of Machining Operations

Introduction of a constitutive material model considering variable carbon content for cutting simulation

Christian Baumann[a]*, Steven P. Mates[b], Stephan Krall[a], Friedrich Bleicher[a]

aInstitute of Production Engineering and Photonic Technologies, TU Wien, Austria
bNational Institute of Standards and Technology, 100 Bureau Drive, Gaithersburg, MD, USA

* Corresponding author. Tel.: +4315880131180. *E-mail address:* christian.baumann@tuwien.ac.at

Abstract

Carbon steels show complex strain hardening and dynamic strain aging effects under high plastic strains, high strain rates, high temperatures and high heating rates, and thus a sufficiently complex constitutive model is needed to capture this behavior. Carbon content in such steels (e.g., AISI 1018, 1045, 1075) influences strength and hardening as well. A recently-developed material model for 1045 steels was therefore modified to capture the effect of carbon content on the material response. The model can also capture time-dependent plastic response associated with interrupted austenite transformation under short (sub-second) heating times, for the simulation of machining operations.

Keywords: Machining, cutting, material, modelling, carbon content

1. Introduction and objective

In production engineering, numerical simulations are relied upon to understand how the behavior of real materials (as opposed to idealized materials) influences material processing technology and performance. Great improvements in the understanding of machining processes have been achieved in the last decade using ever-more-realistic numerical simulations. However, improved simulation accuracy is still needed to enable predictions that can be used to optimize material removal rate, cutting efficiency and tool life without extensive experimentation [1, 2]. In machining, materials are subjected to high plastic strains, high strain rates along with high temperatures and heating rates. These conditions, which can involve strain rates up to 10^6 s^{-1}, temperatures up to and beyond 1000 °C and heating rates exceeding 1000 °C/s, are well beyond ordinary laboratory testing capabilities. The lack of material behavior knowledge under such conditions is a recognized technology barrier [3]. Many attempts to explore the influence of complex material behavior on cutting

mechanics through advanced material modelling have been documented [2, 3, 4]. However, predicting all aspects of the process (forces, temperatures, chip morphologies, etc.) remains elusive and motivates the present work.

Carbon steel behavior is particularly complex compared to many other metals. One important effect included in sophisticated machining models of ferrite-pearlite steels is dynamic strain aging (DSA), which is believed to cause the "blue brittleness" effect in machining, where the steel becomes stronger and less ductile under certain conditions of temperature and strain rate [5, 6].

Another important effect is the austenite transformation on heating, which when followed by rapid cooling of the chips and workpiece surface results in complex mixed microstructures consisting of ferrite-pearlite, bainite and/or martensite [7]. Dynamic recrystallization is yet another effect that is suspected to influence the grain size and surface hardness in cold or dry machining in some steels [3]. It has also been observed in chips at moderate cutting velocities when machining strong martensitic steels [8].

The influence of heating rate and heating time on austenite transformation in ferrite-pearlite steels has been well studied, in connection with steel processing research and welding research. Cementite (Fe$_3$C), the primary strengthening precipitate in plain carbon steel, becomes unstable above the A1 temperature, between 700 °C and 730 °C depending on composition. Pearlite colonies, which are alternating plates of cementite and ferrite, decompose into austenite above A1. Austenite nucleates within pearlite colonies and once they are consumed, a second stage of slower austenite growth occurs into the remaining ferrite [9]. Because heating times in machining are well below one second, it is rather likely that carbon steel deviates significantly from equilibrium flow stress behavior wherever temperatures exceed A1. In high-speed machining of 1045 steel (300 m/min cutting speed), while temperatures are limited to about 400 °C in the primary shear zone, they can greatly exceed A1 in the secondary shear zone along the rake face, as measured by thermocouples [10] and infrared thermography [11].

The complex behavior of carbon steel has been measured recently using an electrically-heated Kolsky bar technique at the National Institute of Standards and Technology (NIST) [12]. Uni-axial compression measurements on three hypo-eutectoid ferrite-pearlite steels with increasing carbon content (American Iron and Steel Institute (AISI) grades 1018, 1045 and 1075) have demonstrated carbon-dependent thermal softening and strain hardening along with DSA and time-dependent phase transformation above A1 [13, 14] with high temperature resolution and under rapid heating. The complex plastic behavior revealed in this study and also in previous studies [15, 16] cannot be captured by general-purpose plasticity models (e.g., Johnson-Cook (JC) [17] shown in Equation (1), Zerilli-Armstrong (ZA) [18], or power law (PL) model [19]) with too few degrees of freedom. While these powerful models show broad agreement with many metals, they must be modified to capture the complex behavior of real materials as revealed by high-temperature-resolution experiments (Figure 1), such as strain rate modified strain hardening, DSA, phase transformations, and the like, as for example in metal cutting research [20].

A new material model was developed and tested to capture the detailed behavior of 1045 steel revealed by the recent pulse-heated Kolsky bar experiments [21, 22]. The model is based on the Preston-Tonks-Wallace (PTW) dynamic plasticity model [23] and employs Voce strain hardening [24], which has enough flexibility to capture the complex strain hardening behavior over wide ranges of temperature and strain rate. In this paper, this model is extended to cover other hypoeutectoid carbon steel compositions (AISI 1018 and 1075) for which high-resolution data are also available, to capture the effect of carbon content on the material behavior for machining simulations. This new carbon-content-dependent model is used to simulate machining experiments recently performed on AISI 1018 and 1045 steels. The influence of carbon content on heating rate effects associated with phase transformation above A1 will be reported on in future work.

$$\sigma = (A + B\varepsilon^n)\left(1 + C \ln\frac{\dot{\varepsilon}}{\dot{\varepsilon}_{ref}}\right)\left(1 - \left(\frac{T - T_{ref}}{T_m - T_{ref}}\right)^m\right) \quad (1)$$

2. Material modelling of hypo-eutectoid carbon steels

The carbon steel model defines a temperature (T) and strain rate (γ) dependent yield (τ_y) and saturation (τ_s) flow stress as follows:

$$\frac{\tau_y}{G(T)} = \left\{ y_0 - (y_0 - y_\infty)erf\left[k\frac{T_K}{T_{m,K}}\right]\right\} \cdot \left(1 + C \ln\frac{\dot{\gamma}}{\dot{\gamma}_0}\right) \quad (2)$$

$$\frac{\tau_s}{G(T)} = \left\{ s_0 - (s_0 - s_\infty)erf\left[k\frac{T_K}{T_{m,K}}\right]\right\} \cdot \left(1 + C \ln\frac{\dot{\gamma}}{\dot{\gamma}_0}\right) \quad (3)$$

Voce hardening is calculated by combining the yield and saturation stresses along with a hardening modulus, θ:

$$\frac{\tau}{G(T)} = \frac{\tau_y}{G(T)} + \int_0^\gamma \theta \frac{\tau_s - \tau}{\tau_s - \tau_y} d\gamma \quad (4)$$

$G(T)$ is the temperature-dependent shear modulus, T_K and $T_{m,K}$ are current temperature and melting temperature in K, respectively, and y_0, y_∞, s_0, s_∞, k, C, $\dot{\gamma}_0$ and θ are fitting parameters. τ and γ denote shear stress and shear strain, respectively, which convert to normal stress and normal strain via $\sigma = \sqrt{3}\tau$ and $\varepsilon = \gamma/\sqrt{3}$

The strain rate dependence is adapted from the work of Vural et al. which shows that the strain rate sensitivity of low carbon steel increases at high strain rates [25]. The strain rate and temperature dependent DSA behavior is captured by modifying the yield, saturation and hardening behavior with a Gaussian function. An example of the yield stress modification is given below. Similar expressions are used to modify τ_s and θ.

$$\tau_{y,MOD} = \tau_y + \tau_{y,DSA} \quad (5)$$

$$\frac{\tau_{y,DSA}}{G(T)} = F(\dot{\gamma})\frac{\tau_{y,0,DSA}}{G(T)} exp\left[-\frac{\left(T - T_\mu(\gamma)\right)^2}{\delta^2}\right] \quad (6)$$

$$F(\dot{\gamma}) = 0.65 + 0.031 \ln\left(\frac{\dot{\gamma}}{\sqrt{3}}\right); T_\mu(\dot{\gamma}) = 414 + 25.668 \ln\left(\frac{\dot{\gamma}}{\sqrt{3}}\right) \quad (7)$$

Here, $\tau_{y,0,DSA}$ and δ are additional fitting parameters. Equations (7) capture the effect of strain rate on the mean temperature and magnitude of DSA strengthening. They are determined using literature data [21]. Austenite transformation is handled by fitting data above the A1 temperature separately. The influence of carbon content is included using quadratic dependencies for the yield and saturation stresses and the thermal softening coefficient on weight percent carbon (% C), and linear dependencies on the strain hardening modulus and the DSA saturation stress on % C, e.g.,

$$y_0 = a \, (\% \, C)^2 + b \, (\% \, C) + c \quad \text{(same for } s_0, k) \quad (8)$$

$$\theta = a \, (\% \, C) + b \quad \text{(same for } \tau_{s,0,DSA}) \quad (9)$$

The strain rate sensitivity coefficients are unchanged from the one used previously for 1045 steel [21]. The resulting model uses 20 fitting parameters to capture AISI 1045 steel behavior up to 1000 °C, strains up to 0.6 and strain rates up to 20 000 1/s, and 21 additional parameters to express carbon content dependencies for steels ranging from 0.18 % C to 0.75 % C for material behavior, with separate sets of model coefficients for behavior below and above the A1 temperature. All parameters for the model implementation used in this paper are listed in Table 1.

Table 1. Modified PTW plasticity model (m-PTW) coefficients for hypoeutectoid carbon steels (AISI 1018, 1045 and 1075). A1 = 706.31 + 26.14 × (% C). All temperatures in this table are in °C.

	y_0	y_∞	s_0	s_∞	k	θ
(T < A1)	4.06e-3	0.0	7.26e-3	8.04e-7	0.748	0.0100
(T > A1)	5.74e-3	0.0	1.61e-3	1.83e-4	1.32	0.0168
	$\tau_{y,0,DSA}/G(T)$		$\tau_{s,0,DSA}/G(T)$		θ_{DSA}	δ [°C]
m-PTW	3.15e-7		0.00342		0.0371	113.3
G(T) [GPa]	$82.218 - 0.012085T - 5.7217 \cdot 10^{-5}T^2 + 2.6635 \cdot 10^{-8}T^3$					
	C		$\dot\gamma_0$ [1/s]		T_m [°C]	
$\dot\gamma \leqslant 166$	$0.0177\dot\gamma^{-0.0148}$		5.0e-6		1432	
$\dot\gamma > 166$	$0.0539\dot\gamma^{-0.0555}$		1.65		1432	
	a		b		c	
y_0 (T < A1)	-0.000459		0.00177		0.00344	
y_0 (T > A1)	-		0.000341		0.00561	
s_0 (T < A1)	0.00445		-0.00403		0.00840	
s_0 (T > A1)	-		0.00345		0.0127	
k (T < A1)	2.15		-3.46		1.98	
k (T > A1)	-		-0.227		1.40	
θ (T < A1)	-		0.0216		-6.62E-07	
θ (T > A1)	-		0.0126		0.0102	
$\tau_{s,0,DSA}$	-		-0.00293		0.00523	

The model fit is plotted against 1018 and 1045 data at a plastic strain of 0.1 in Figure 1. For comparison, an unmodified JC model is fit to the same data sets (excluding the DSA region to better fit low and high temperature flow stress data), highlighting the increased ability to fit carbon steel behavior of the new model compared to this widely-used but simple general-purpose plasticity model. The unmodified JC model parameters are shown in Table 2. The fit uses $T_0 = 23$°C, $T_m = 1432$°C and $\dot\varepsilon_{p0} = 1$ s^{-1}.
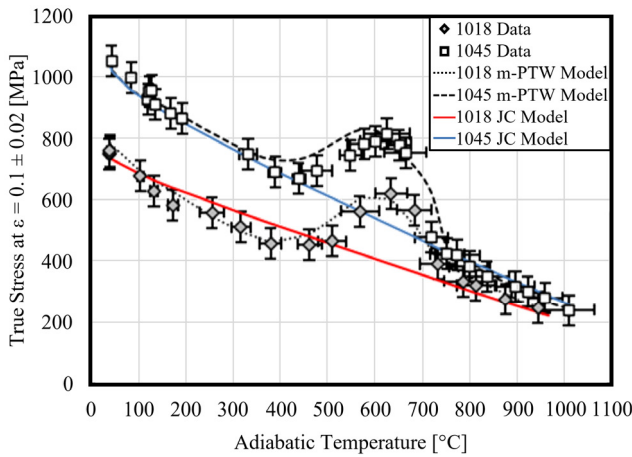

Figure 1. Flow stress data and model fits for 0.1 plastic strain at strain rates of order 3500 s^{-1} (strain rate varies slightly with material strength) for AISI 1018 and 1045 carbon steels. JC model fits (ignoring DSA effects) to 1018 and 1045 data are shown for comparison.

Table 2. Johnson-cook plasticity model coefficients for AISI 1018 and 1045.

	A	B	C	n	m
AISI 1018	550	434	0.0223	0.5226	0.8292
AISI 1045	200	830	0.0329	0.1242	0.8577

In [21] validation curves for several strain rates of 1045 are given. Two different model fits at different strain rates are plotted for 1018 in Figure 2. An object of the present study is to determine to what extent the increased fidelity of the new carbon steel model alters or improves the agreement between cutting simulations and experiments. Figure 2 is presented to highlight an important issue regarding the lack of knowledge of material behavior relevant to machining, namely the behavior at large plastic strains (>2). Dynamic compression test data are generally limited to strains of about 0.5 due to friction effects, although incremental testing has been done out to strains as high as 1.0 [15]. Model fits derived from such data must therefore be extrapolated to high strains to simulate machining processes. As Figure 2 demonstrates, extrapolations can vary widely depending on the nature of the strain hardening models used, even when the model coefficients are obtained by fitting the same data. Strain hardening behavior is known to significantly influence cutting force and chip thickness predictions [26, 27]. Strain hardening at large strains has been modified in some machining models using a strain hardening cut-off parameter [10]. In the new model described here, the strain hardening at large strains is limited by the saturation stress hardening model concept. The limited strain hardening capacity of the m-PTW model explains why its extrapolated flow curves drop below the extrapolated JC model flow curves in Figure 2, as the latter model allows unlimited strain hardening. Strain hardening is also affected by the material's temperature sensitivity. We note that the current model fit lacks independent experimental confirmation beyond the maximum strains in the compression test data, but this issue is currently being addressed and will be reported on soon.
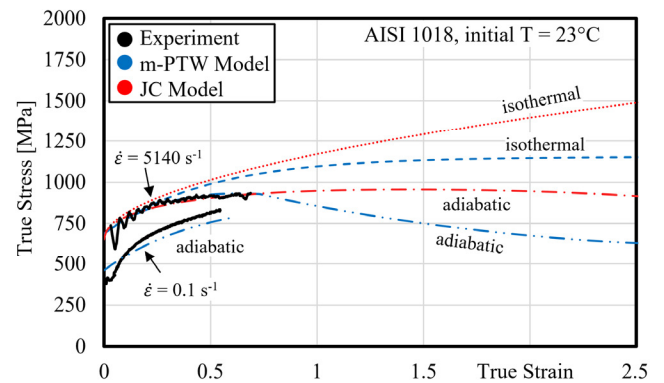

Figure 2. Comparison of new model against the Johnson-Cook model fit to AISI 1018 data extrapolated to high plastic strains highlighting significant differences in strain hardening behavior.

3. Implementation in FEM-simulation

A thermo-mechanically coupled finite element analysis of the orthogonal cutting process was performed using DEFORM 2D[1] v12.0.1 to predict machining forces for hypo-eutectoid carbon steels (AISI 1018 and 1045), machined with TiAlN coated carbide tools. Orthogonal cutting simulations were performed for different combinations of feed rate (f) and cutting speed (v$_c$) to evaluate the entire range of available experimental conditions. Multiple development stages were required to establish a simulation model that would make accurate predictions. A sensitivity analysis of element size, interference depth, length of cut, and step time was carried out, and the findings were applied in the final simulation model.

The model was created using the DEFORM 2D cutting preprocessor assuming a plane strain idealization of the cutting conditions. The workpiece (5 mm long by 2 mm deep) is defined as a plastic body and is meshed using (≈ 2500) linear

quadrilateral elements with 4 integration points, as shown in Figure 3a. A strategy of mesh grading, by using mesh windows is applied to the workpiece. The workpiece consists of three areas with different element edge sizes. A dense mesh is maintained in the cutting zone, where the edge size ranges from 6 µm at the cutting zone to 200 µm at the fixed bottom surface. An interference depth of 3 µm is implemented as an automatic remeshing criterion for the workpiece. The chip morphology was modeled as continuous. For the tool, two windows are defined, whose elements range from 20 µm at the cutting edge to 30 µm outside the cutting zone. The cutting tool was defined as a rigid body and meshed with 1150 linear quadrilateral elements with 4 integration points. The boundary conditions of the generated model are depicted in Figure 3a. The workpiece far from the cutting zone is maintained at ambient temperature ($T_0 = 20$ °C) while the initial tool temperature is fixed at 650 °C (determined by measurement) to emulate steady cutting conditions.

The new carbon-content-dependent steel material model was implemented in DEFORM by creating tables, using a Python code, of isothermal flow stress versus temperature and strain rate for the carbon concentration of interest (0.18 % and 0.48 % for this work), as shown schematically in Figure 3b. The plasticity model is implemented with von Mises yield behavior and isotropic hardening. The material model implementation within DEFORM was validated by performing simulations of compression tests at different strain rates and temperatures.
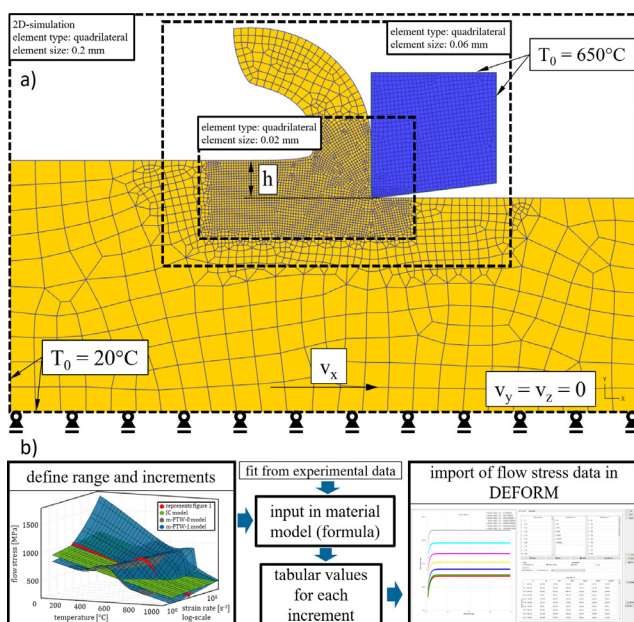

Figure 3. a) Boundary conditions and b) Implementation of flow stress data.

Temperature-dependent thermophysical properties, such as Young's modulus, heat capacity, density, thermal conductivity, etc., were calculated based on the CalPhad method using JMatPro V11. The elastic and thermal properties of the TiAlN-coated carbide tool were taken from the DEFORM tool material library.

The Coulomb friction model employed here is linearly dependent on cutting speed, as shown in Figure 4. Friction data for AISI 1045 come from tests performed at IFT TU Wien as part of the CIRP working group activity. The AISI 1018

friction data are from Hong et al [28], although the coefficients were reduced by 15% due to the different tool coating used (TiAlN instead of TiN) and because the inserts were only used for short periods [29].
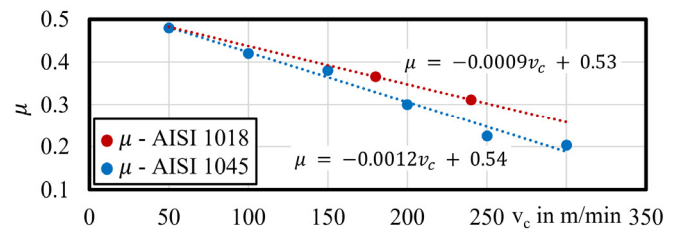

Figure 4. Coulomb friction coefficients for AISI 1018 and AISI 1045.

4. Comparison of Simulations and Experiments

4.1. Experimental setup

Dry orthogonal cutting experiments were conducted using a DMG-MORI CTX gamma mill - turning center, equipped with a dynamometer (Kistler type 9129AA) for measuring cutting force (F_c) and feed force (F_f) to compare with the simulation results. The test setup is depicted in Figure 4.

A full factorial design of experiment was used, comprising 3 levels of feed rate (f) in the range of 0.1 mm/rev to 0.3 mm/rev and 3 levels of cutting speed (v_c) in the range of 200 m/min to 300 m/min. Cutting was performed with TiAlN coated carbide inserts SCMW 120408 (corner radius $r_\beta = 0.8$ mm), grade P25. The cutting inserts have a rake angle of $\gamma = 0°$ and a cutting-edge radius $r_\beta = 30$ µm. Disc-shaped workpiece samples were cut from annealed bar stock of 100 mm diameter for AISI 1018 and 80 mm diameter for AISI 1045. The workpiece disks had a common thickness of 4 mm. The specimens were placed on a mounting adaptor, which was fixed in a three-jaw chuck. Based on previous experimental work, the depth of cut was varied from 1 mm at high cutting speeds up to 2 mm for the lowest cutting speed to achieve steady-state cutting and minimal tool wear. The tool inserts were also changed during the experiments to limit effects resulting from tool wear.

The total uncertainty in force measurement is ± 25 N (one standard deviation) and was determined through numerous experiments using the same experimental setup.
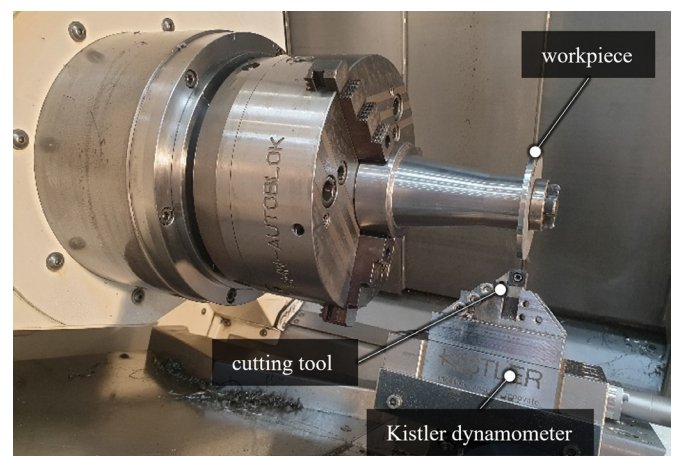

Figure 5. Experimental test setup for orthogonal cutting.

4.2. Results

Two-dimensional simulation results are compared against experimental data in Figures 6 through 9. Normalized force values (error bars being one standard deviation) are calculated for a reference width of cut of 1 mm to compare simulations and cutting measurements, which have a 4 mm width of cut, (b). Figure 6 plots cutting force and Figure 7 feed force measurements of AISI 1018 compared with the simulations. All simulation results show decreasing cutting forces at increased cutting speeds and lower feed rates, in accord with experiment. It can be seen that the cutting forces agree well for f = 0.3 mm and all cutting speeds, but the predicted force falls more quickly in the simulation than otherwise seen in the experiments. Feed forces are under-predicted for all conditions.
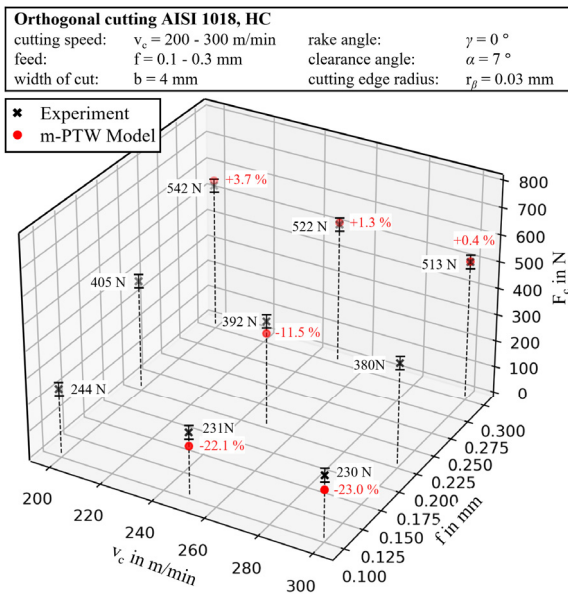

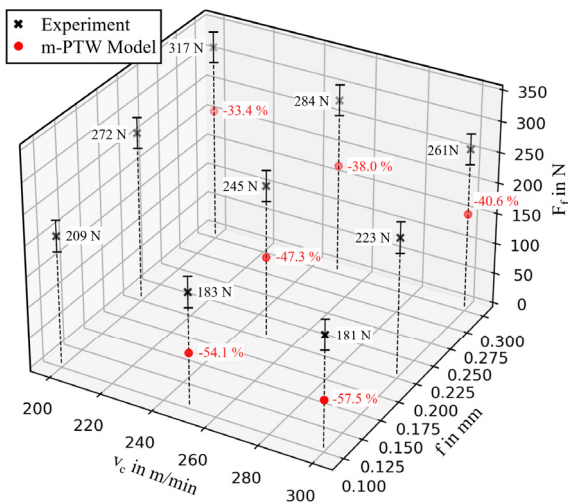Figure 6. Experimental and simulation results of normalized F_c of AISI 1018.

Figure 7. Experimental and simulation results of normalized F_f of AISI 1018.

In Figure 8 and Figure 9 the cutting force and feed force measurements of AISI 1045 are compared with the 2D simulations. Again, cutting forces are well predicted at all cutting speeds for f = 0.3 mm, but this agreement worsens with decreasing feed rates. Feed forces are again low compared to

experiments under all conditions, which is usually observed regardless of the material model used [26].
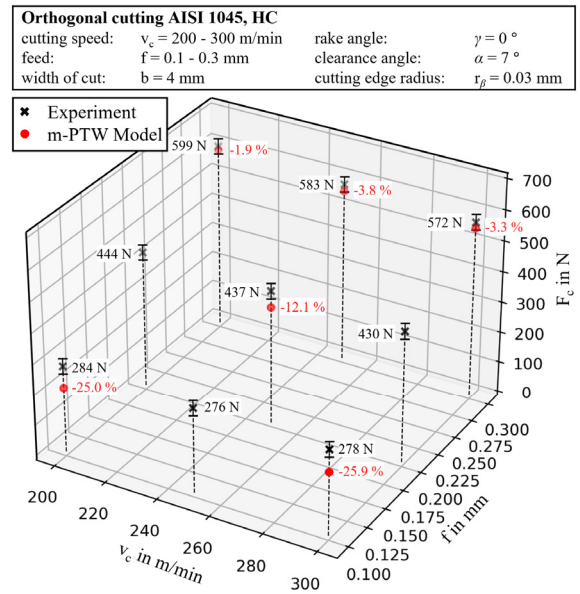

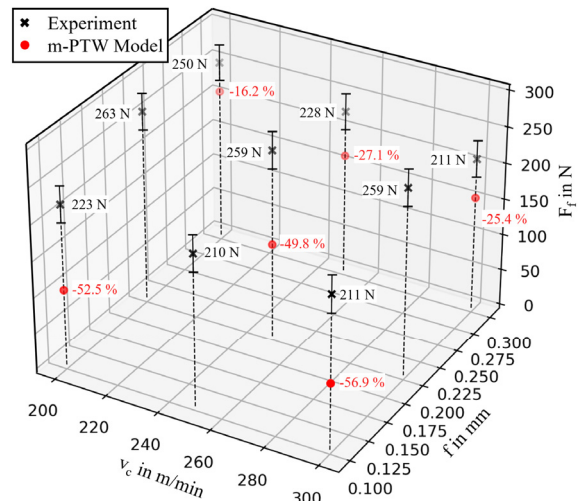Figure 8. Experimental and simulation results of normalized F_c of AISI 1045.

Figure 9. Experimental and simulation results of normalized F_f of AISI 1045.

In general, it can be said that based on the simulation results of the cutting and feed force, the carbon-dependent model provides reasonable cutting force predictions from 2D finite element simulations for different low carbon steels (1018 and 1045), with better agreement at high feed rates. The simulations indicate an average increase in F_c of 8.2 % from 1018 to 1045 steel compared with an experimental increase of 11.6 % for the same cutting conditions. The simulations indicate larger differences between 1018 and 1045 at lower feed rates, in agreement with the experimental trend. F_f changes very little with carbon content in the simulations except at the lowest feed and highest speed condition where it increases by 15 % for 1045. Experimentally F_f increases at low feed rates but decreases at high feed rates as the carbon content goes up. Feed force predictions were generally low, as expected from experience of an earlier study [22]. Good cutting force predictions with this model on 1045 steel have been attributed partly to the Voce strain hardening model, with more rapid

strain softening at high strains compared to the JC model [22]. This model is now extended to include carbon steels having different carbon content.

5. Conclusions

The use of a carbon-content-dependent material model that considers effects of high heating rate and complex strain hardening shows generally good agreement with orthogonal cutting experiments at high feed rates for AISI 1018 and 1045 carbon steels with varying carbon content as a model input parameter. The model captures the increase in cutting force as the steel strength (carbon content) increases, while the feed force changes very little with carbon content in the simulations in contrast to the experiments. Feed and cutting force predictions at lower feed rates are low for both materials. Higher deviation from the experiment with decreasing feed rate are seen to be dependent on the friction model [30]. Feed forces are usually under-predicted in finite element simulations despite wide differences in the material models and friction models used [31, 32]. The reason for the deviation in the feed force could be explained by the simplification of the simulation model. The simulation does not include the elastic deformation of the workpiece and therefore the simulated feed forces may be lower compared to experiments [32]. Good agreement of cutting forces at high feed rates has been attributed to the increased adiabatic strain softening enabled by the Voce strain hardening model, which produces lower stresses at large strains compared to power law strain hardening used in the JC model. Independent experimental verification of the large-strain behavior of carbon steel under dynamic loads is needed to determine which strain hardening model is appropriate.

Further investigations with a comparison to a JC model fit to the same data for both materials with regard to the chip geometry are planned. Additional aspects such as the friction modelling has to be considered for further tests, to evaluate the influences of the frictional behavior on F_f.

Acknowledgement

References

[1] Tlusty J. Manufacturing processes and equipment. Prentice-Hall; 2000

[2] Trent EM, Wright PK. Metal cutting. Butterworth-Heinemann; 2000

[3] Arrazola PJ, Özel T, Umbrello D, Davies M, Jawahir IS. Recent advances in modelling of metal machining processes. CIRP Ann Manuf Technol 2013; 62/2:695–718

[4] Childs THC, Maekawa K, Obikawa T, Yamane Y. Metal machining: theory and applications. Butterworth-Heinemann; 2000

[5] Warnecke G, Oh J-D. A new thermo-viscoplastic material model for fnite-element-analysis of the chip formation process. CIRP Ann Manuf Technol 2002; 51/1:79–82

[6] Dirikolu MH, Childs THC, Maekawa K. Finite element simulation of chip flow in metal machining. Int. J. Mech. Sci. 2001; 43/11:2699–2713

[7] Schulze V, Michna J, Zanger F, Pabst R. Modeling the process-induced modifcations of the microstructure of work piece surface zones in cutting processes. Adv Mater Res 2011; 223:371–380

[8] Duan CZ, Zhang LC. Adiabatic shear banding in AISI 1045 steel during high speed machining: mechanisms of microstructural evolution. Mater. Sci. Eng. A 2012; 532:111–119

[9] Speich GR, Demarest VA, Miller RL. Formation of Austenite During Intercritical Annealing of Dual-Phase Steels. Metallurgical Transactions A 1981; 12A:1419-1428.

[10] Childs THC, Otieno AW. Simulations and experiments on machining carbon and low alloy steels at rake face temperatures up to 1200°C. Mach. Sci. Technol. 2012; 16/1:96-110

[11] Saez-de-Buruaga M, Soler D, Aristimuño PX, Esnaola JA, Arrazola PJ. Determining tool/chip temperatures from thermography measurements in metal cutting. Appl. Therm. Eng. 2018; 145:305-314

[12] Mates SP, Rhorer R, Whitenton E, Burns T, Basak D. A pulse-heated Kolsky bar technique for measuring the flow stress of metals at high loading and heating rates. Exp Mech 2008; 48:799-807

[13] Mates SP, Vax E, Rhorer RR, Stoudt MR. Dynamic flow stress behavior of hypo-eutectoid ferrite-pearlite steels under rapid heating. J. Dyn. Behav. Mater. 2020; 6/2:246-265

[14] Mates S, Stoudt M, Gangireddy S. Measuring the influence of pearlite dissolution on the transient dynamic strength of rapidly heated plain carbon steels. JOM 2016; 68/7:1832-1838

[15] Shirakashi T, Maekawa K, Usui E. Flow Stress of Low Carbon Steel at High Temperature and Strain Rate (Part 1) - Propriety of Incremental Strain Method in Impact Compression Test with Rapid Heating and Cooling Systems. Bull. Japan Soc. Prec. Engg. 1983; 17/3:161-166

[16] Jaspers SPFC, Dautzenberg JH. Material Behavior in Conditions Similar to Metal Cutting: Flow Stress in the Primary Shear Zone. J Mater Process Technol 2002; 122:322-33

[17] Johnson GR, Cook WH. A constitutive model and data for materials subjected to large strains, high strain rates, and high temperatures. Proc 7th Int Sympo Ballistics 1983; 541-547

[18] Zerilli FJ, Armstrong RW. Dislocation-mechanics-based constitutive relations for material dynamics calculations. Journal of Applied Physics 1987; 61/5:1816-1825

[19] Marusich TD, Ortiz M. Modeling and simulation of high-speed machining. Int J Numer Meth Eng 1995; 38/21:3675-3694

[20] Childs THC. Towards simulating built-up-edge formation in the machining of steel. CIRP J Manuf Sci Technol 2011; 4/1:57-70

[21] Mates SP, Li S-Y. Dynamic Plasticity Model for Rapidly Heated 1045 Steel Up to 1000 C. J Res Natl Inst Stand Technol 2021; 126: 1-17

[22] Bleicher F, Baumann C, Krall S, Mates SP, Herzig S, Alder T, Herzig N. Considering the influence of heating rate, complex hardening and dynamic strain aging in AISI 1045 machining: experiments and simulations. CIRP Annals 2021; 70/1:49-52

[23] Preston DL, Tonks DL. Model of plastic deformation for extreme loading conditions. J. Appl. Phys. 2003; 93/1:211-220

[24] Voce E. The relationship between stress and strain for homogeneous deformation, J. Inst. Metals 1948; 74:537–562

[25] Vural M, Ravichandran G, Rittel D. Large strain mechanical behavior of 1018 cold-rolled steel over a wide range of strain rates. Metall Mater Trans A 2003; 34:2873-2885

[26] Childs THC. Revisiting flow stress modelling for simulating chip formation of carbon and low alloy steels, Procedia CIRP 2019; 82:26-31

[27] Wielki N, Kuschel S, Sölter J. A Comparative Study of the Influence of the Strain-Hardening in Chip Formation Simulations using Different Software Packages. Procedia CIRP 2019; 82:43-46

[28] Hong SY, Ding Y, Jeong J. Experimental evaluation of friction coefficient and liquid nitrogen lubrication effect in cryogenic machining. Mach. Sci. Technol. 2002; 6/2:235-250

[29] Liu A, Deng J, Cui H, Chen Y., Zhao J. Friction and wear properties of TiN, TiAlN, AlTiN and CrAlN PVD nitride coatings. Int J Refract Hard Met 2012; 31:82-88.

[30] Haglund AJ, Kishawy HA, Rogers RJ. An exploration of friction models for the chip–tool interface using an Arbitrary Lagrangian–Eulerian finite element model. Wear 2008; 265/3–4:452-460

[31] Filice L, Micari F, Rizzuti S, Umbrello D. Dependence of machining simulation effectiveness on material and friction modelling, Mach. Sci. Technol. 2008; 12/3:370-389

[32] Shi B, Attia H. Modeling the thermal and tribological processes at the tool-chip interface in machining. Mach. Sci. Technol. 2009; 13/2:210-226